Taylor & Francis
Taylor & Francis Group

Canadian Metallurgical Quarterly
The Canadian Journal of Metallurgy and Materials Science

ISSN: 0008-4433 (Print) 1879-1395 (Online) Journal homepage: https://www.tandfonline.com/loi/ycmq20

# Recyclability assessment of Al 7075 chips produced by cold comminution and consolidation using spark plasma sintering

P. Hendrickx, M. M. Tünçay & M. Brochu

**To cite this article:** P. Hendrickx, M. M. Tünçay & M. Brochu (2016) Recyclability assessment of Al 7075 chips produced by cold comminution and consolidation using spark plasma sintering, Canadian Metallurgical Quarterly, 55:1, 94-103, DOI: 10.1080/00084433.2015.1125094

**To link to this article:** https://doi.org/10.1080/00084433.2015.1125094

# Recyclability assessment of Al 7075 chips produced by cold comminution and consolidation using spark plasma sintering

**P. Hendrickx, M. M. Tünçay and M. Brochu***

A solid-state recycling route for processing aluminium alloy 7075 chips is proposed. This process involves pulverizing the chips using an industrial scale comminution line to produce a broad particle size distribution of granulated products and powders. Upon sieving, the −140 mesh fraction of the pulverised material was consolidated by spark plasma sintering into fully dense compacts, i.e. >99%. The properties of the pulverised powders and compacts were compared to commercially available aluminium alloy 7075 powder used in industrial press-sinter applications. The comminution line produced powder particles which possessed a 7·9 ± 0·6-nm thick native oxide layer with adhering exogenous contaminants, and aluminium oxide particles dispersed throughout the powder. The presence of the oxide layer and exogenous contaminants was found to be deleterious to the powder consolidation and mechanical properties. A flexural strength and strain and hardness of 94·7 ± 7·2 MPa, 2·1 ± 0·3% and 69·3 ± 5·2 HV were obtained, respectively.

On suggère une voie de recyclage à l'état solide pour le traitement de copeaux d'alliage d'aluminium 7075. Ce procédé implique la pulvérisation des copeaux en utilisant une ligne de broyage à l'échelle industrielle afin de produire une large distribution de taille de particule de produits granulés et de poudres. Après tamisage, la fraction d'ouverture de maille de -140 du matériel pulvérisé était consolidée par frittage par étincelage au plasma en comprimés complètement denses, i.e. > 99%. On a comparé les propriétés des poudres pulvérisées et des comprimés à la poudre d'alliage d'aluminium 7075 disponible commercialement et utilisée dans les applications industrielles de pressé-fritté. La ligne de broyage produisait des particules de poudre qui possédaient une couche d'oxyde natif de 7.9 ± 0.6 nm d'épaisseur avec contaminants exogènes adhérents, et des particules d'oxyde d'aluminium dispersées à travers la poudre. On a trouvé que la présence de la couche d'oxyde et de contaminants exogènes était nuisible à la consolidation de la poudre et aux propriétés mécaniques. On a obtenu une résistance à la flexion, une déformation et une dureté de 94.7 ± 7.2 MPa, 2.1 ± 0.3% et 69.3 ± 5.2 HV, respectivement.

**Keywords:** Comminution; Spark plasma sintering; Aluminium alloy; Recycling; Oxide dispersion; Powder metallurgy

## Introduction

In the past few years, the issues associated with the recycling of aircraft components has gained growing attention due to the increasing amounts of aircraft reaching their end of life. In that context, the need to develop cost-effective routes to recycle aerospace aluminium alloys from these aerostructures is emerging. Among the major challenges, the process optimisation for comminution and remelting of Al 2xxx, Al 7xxx and blends of alloys is central in the effort to develop a recycling stream aiming towards high-added value revalorised products.[1]

REGAL Aluminum Research Center, Materials Engineering Department, McGill University, 3610 University Street, Montréal, Québec, Canada H3A 0C5

*Corresponding author, email mathieu.brochu@mcgill.ca


Published by Taylor & Francis on behalf of the Institute
Received 15 June 2015; accepted 23 November 2015
DOI 10.1080/00084433.2015.1125094

Particularly, comminution presents the significant advantage of reducing the energy consumption when compared to remelting, further increasing the sustainability of these revalorised products.[2] Moreover, this improved energy efficiency of the process is enhanced with increased material throughput during recycling.[3] During typical Al recycling processes (including remelting operations), approximately 41% of the molten Al does not contribute to the final recycled product and is diverted into process scrap which, in turn, can then be recycled.[4] Besides, remelting-based processes are not recommended for Al turnings and chips recycling as the latter were found to float at the surface of molten Al, thus exhibiting oxidation and losses ranging between 16 and 25%.[5,6] As such, the revalorisation of end-of-life aircraft materials through a complete solid-state approach combining comminution and powder metallurgy (PM) consolidation techniques is attractive as it would reduce the energy consumption and material losses by ~90% when compared to the currently used remelting stream.[7–9]

Comminution is a severe plastic deformation process capable of producing tailored particulate materials with controlled microstructural and particle length scales upon proper process optimisation.[10] It is currently used to some extent, prior to remelting, in the recycling chain of the Al can industry, but its usage serves cascade recycling.[11] Optimizing the comminution process becomes a promising alternative to cascade recycling, mostly since powders presenting characteristics similar to those prepared by conventional milling processes such as reduced particle size, refined microstructure and degree of contamination, can be obtained.[11] During milling, the powder particles undergo extensive deformation leading to significant particle size reduction and possible grain size reduction.[12] The particle size reduction occurs through an increase in dislocation density leading to embrittlement and fracture of the deformed particle. The produced feedstock can subsequently be used in the PM supply chain.

Recently, solid-state recycling approaches aiming at the direct consolidation of recycled Al turnings and chips into end-process products have been studied.[8,9,13] These approaches typically focused on hot extrusion, targeting the production of elongated profiles. Particularly, one study focused on recycling by cold compaction and hot extrusion of Al 7075 alloy chips blended with pure atomised Al acting as a binder to create two-phase materials.[13] The ductility of the extruded material decreased with increasing Al 7075 chip content due to poor Al 7075/Al bonding and the lower ductility of Al 7075.

Spark plasma sintering (SPS) is a recently developed sintering process based on the simultaneous applications of external pressure and high-pulsed current to the powder bed. The combined Joule heating and mechanical loading during sintering contributes to the breakage of the native oxide scale present at the surface of powders which increases the extent of sintering.[14] Therefore, SPS provides an ideal processing route enabling the production of near-net shape parts from feedstock originating from the recycling chain.[15] Unfortunately, a significant knowledge gap currently exists with respect to the SPS of pulverised feedstock and more so, on the specific example of Al 7075. As such, the present work will provide insight on the possible recycling strategy involving comminution of Al 7075 chips followed by SPS processing. The properties of the Al 7075 pulverised powders and compacts were compared to a reference Al 7075 atomised powder to evaluate this recycling strategy.

## Experimental procedures

### Powder fabrication and sampling

The morphology of the starting Al 7075 alloy chips originating from machining operations is presented in Fig. 1, where clear ribbons and strip shapes can be observed. This starting feedstock was milled using a patented cold comminution process involving a Turbo 900/5 Pulverizer (Guidetti Inc.). Comminution of the chips was carried out in air at room temperature in a cylindrical chamber equipped with high-speed rotating steel hammers attached to metal plate rings. The inner wall of the chamber was covered with steel teeth-walled cuirasses. The pulverisation parameters include hammer–wall distance of 10 mm, constant rotational speed of 1800 rev $min^{-1}$ and the ventilation system, used for material transport, was set at 145 Hp. The output of the pulveriser successively passed through cyclones and a two-stage vibratory sieve for separation into specific particle size

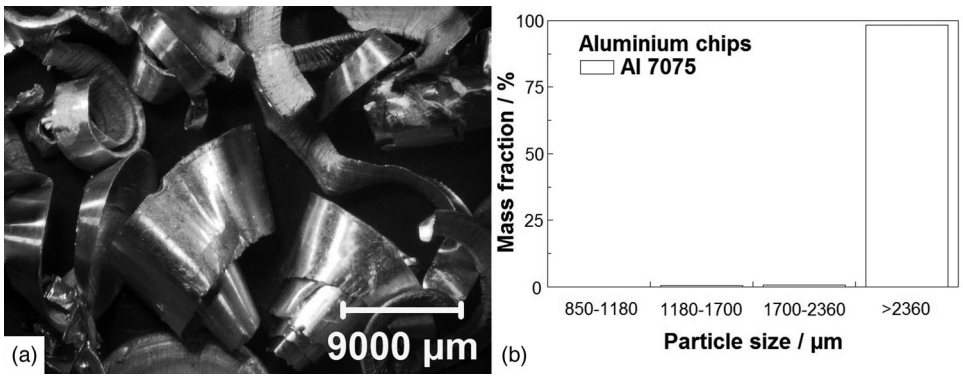


1 *a* Stereoscope micrograph and *b* PSD of the as-received Al 7075 alloy chips

fractions. The upper and lower sieves mesh sizes were 5 and 50 mesh, respectively. Three samples of 100 g from −50 mesh pulverised powders were collected and mixed according to MPIF standard 01, at 0·25*t*, 0·5*t* and 0·75*t* where *t* is the duration of the comminution trials.[16] The collected powder was screened using a −140 mesh laboratory sieve to obtain a typical particle size distribution (PSD) used during powder pressing operations. Powder samples for testing were prepared using a sample splitter. Gas atomised Al 7075 powder, −325 mesh, from Valimet Inc. was used as reference for comparison with the pulverised powder and compacts. The compositions of both the starting chips used for pulverisation and the reference atomised powder determined by inductively coupled plasma optical emission spectroscopy (ICP-OES) are given in Table 1.

## Powder characterisation

The exogenous contamination of the Al 7075 chips, composed of adhering oxide and silicate compounds arising from the plant activities, material storage conditions and *in situ* oxidation, was mechanically separated from the feedstock chips. The content of each compound was quantified by ICP. Three samples were fully digested at 95°C for 2 h in a 3:1 (vol.) $HCl/HNO_3$ acid solution. Hydrofluoric acid (HF) was subsequently added to the solution to ensure complete digestion of the silicon oxide contaminants. Calibration standards of 0·05, 0·5, 5 and 50 ppm were prepared to quantify the contents in K, Ca, Si and Fe of the dissolved contaminants. The emission wavelengths recorded for each element were selected to avoid spectral interferences. Oxygen content analysis of both pulverised and atomised powders was carried out by inert gas fusion (IGF) using a Leco ONH 836 instrument. Three different samples were tested for each powder. The carrier gas was helium with a flow rate of 450 $cm^3\ min^{-1}$. The instrument calibration was performed using a NIST traceable oxygen standard.

The PSD of the starting feedstock was measured according to MPIF standard 05 using laboratory sieves.[16] The PSD of the pulverised and atomised powders were measured using a Horiba LA-920 laser diffraction particle size analyser according to ASTM B822-02.[17] Each powder was dispersed in isopropyl alcohol and the shape correction factor used was identical for both powders. PSD and cumulative frequency curves including the $D_{10}$, $D_{50}$ and $D_{90}$ values are reported.

Scanning electron microscopy (SEM) was used to observe the morphology of the pulverised and atomised powders and the cross-section of the pulverised powder compact, using a Hitachi SU3500 SEM microscope. The SU3500 microscope was coupled with Energy Dispersive Spectroscopy (EDS) capabilities, which was used to highlight the presence of embedded exogenous contamination within the sintered materials.

Metallographic sample preparation included mounting in conductive resin, grinding using SiC paper and polishing with 6 and 1 μm diamond suspensions followed by colloidal silica suspension. Microstructures were revealed by chemical etching using Keller's reagent (1 mL HF, 1·5 mL HCl, 2·5 mL $HNO_3$ and 95 mL $H_2O$). The samples were immersed for 25 s, followed by dipping in nitric acid to reveal the grains.

High-resolution transmission electron microscopy (HRTEM) observations were carried out using a FEI Tecnai G2 F20 transmission electron microscope operated at 200 kV, to determine the passivation layer thickness on both types of powders. The samples were deposited on carbon coated copper grids. The passivation layer thickness reported for each powder was the average of 50 measurements, collected over 10 TEM micrographs per powder. Selected area electron diffraction (SAED) patterns and EDS linescans were used to highlight the transition from the powder particle matrix to the oxide passivation layer. On the other hand, bright-field (BF) and dark-field (DF) micrographs combined with SAED patterns were also used to determine the presence of refined grains in the pulverised powder.

## Spark plasma sintering and compact characterisation

Both the pulverised and atomised powders were consolidated using a Thermal Technology LLC 10-3 SPS press into 38 mm diameter and 7 mm thick compacts in graphite dies. Each powder was heated up to 375°C using a heating rate of 100°C $min^{-1}$ and held for 5 min, followed by subsequent furnace cooling down to room temperature. A preload pressure of 4·7 MPa was initially applied at room temperature and was ramped up to 50 MPa simultaneously to the temperature profile, and held until completion of the sintering cycle. The sintering experiments were carried out in triplicates for each powder. A mechanical vacuum of $6{\cdot}0 \times 10^{-2}$ torr or below was maintained in the sintering enclosure for the duration of the sintering trials.

Density of the sintered compacts was evaluated using the Archimedes principle according to MPIF standard 42.[16] Reported grain size distributions (GSD) were obtained by measurements of the equivalent spherical diameter collected from over 300 grains from optical micrographs. GSD of the sintered compacts were established in accordance to this procedure and the characteristic $G_{10}$, $G_{50}$ and $G_{90}$ values are reported.

The mechanical behaviour of the compacts was evaluated through microhardness and three-point flexural testing. A Clark Microhardness (CM-100AT) instrument equipped with a Vickers indenter using 50 gf load was used in conjunction with an optical microscope to measure the hardness. Optical micrographs of typical indents in the sintered compacts of pulverised and atomised powders were reported. The hardness measurements obtained were the average of 10 indentations, according to MPIF standard 51.[16]

Flexural strength and strain of the compacts were tested by three-point bending using a Tinius Olsen H25K-S Instron with a crosshead displacement speed of 5 mm $min^{-1}$, as per MPIF standard 41.[16] The dimensions of the bending samples were 38 mm × 7 mm × 2·5 mm. The flexural strength $\sigma_{flex}$ and strain $\varepsilon_{flex}$ were calculated

**Table 1 Chemical compositions of the Al 7075 atomised powders and chips, determined by ICP-OES**

| Wt-% | Si | Mn | Cr | Cu | Fe | Mg | Zn | Al |
|---|---|---|---|---|---|---|---|---|
| Al 7075 gas atomised powder | 0·13 | 0·02 | 0·19 | 1·54 | 0·17 | 2·25 | 5·4 | Bal |
| Al 7075 chips | 0·03 | 0·02 | 0·02 | 2·2 | 0·06 | 1·8 | 6·6 | Bal |

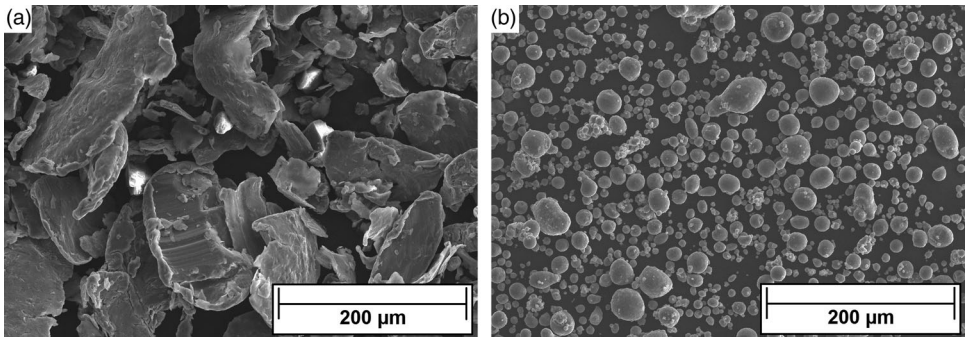


**2 SEM micrographs showing the morphologies of *a* pulverised and *b* gas atomised Al 7075 powders**

from force–displacement recordings and sample geometry, for each sintered material using equations (1) and (2), respectively:[18]

$$\sigma_{\text{flex}} = \frac{3PL}{2bd^2}, \quad (1)$$

$$\varepsilon_{\text{flex}} = \frac{6Dd}{L^2}, \quad (2)$$

where $P$ is the applied force, $L$ is the gauge length, $b$ is the sample width, $d$ is the sample thickness and $D$ is the sample deflection. Each reported value is an average of three samples. The fracture surfaces of the pulverised and atomised sintered compacts were observed through SEM as well.

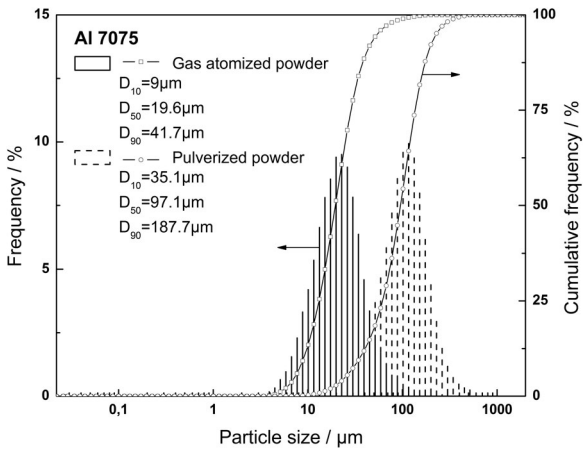


**3 PSD and cumulative frequency curves including $D_{10}$, $D_{50}$ and $D_{90}$ values of the pulverised and gas atomised Al 7075 powders**

# Results and discussion

## Powders

The pulverised powders, shown in Fig. 2*a*, displayed an irregular platelet and flake morphology, while the Al 7075 atomised powder of Fig. 2*b* exhibited typical gas atomised spherical particles. The pulverised powders present features similar to powders processed either by ball milling or attrition. During such processes, it has been reported that initially spherical powder particles undergo extensive deformation and gradually flatten into platelets and flakes as the milling duration increases.[12] Ultimately, the platelets and flakes particles break down into finer irregular particles. Collision and impacts events cause significant accumulation of dislocations within the powder particles until dislocations saturation is reached. At this stage, fracture of the particle into finer strain-hardened particles occurs.[12] The present comminution process is, however, orders of magnitude faster than these conventional milling processes. The chips typically reside ~150 s in the comminution chamber while powder milling is usually carried out for up to 8 h in attritor mills and 40 h in planetary ball mills.[12] As such, the powder fracturing mechanism is incomplete and the dislocation-saturated particle state is never achieved, explaining the pulverised powder morphology presented in Fig. 2*a*.

The PSD of the Al 7075 pulverised and atomised powders are shown in Fig. 3. The atomised powder PSD ranged from 4 to 200 µm. The PSD of the pulverised powder ranged from 9 to 452 µm and is significantly larger and broader than its atomised counterpart.

The microstructural evolution taking place upon comminution of the feedstock chips is highlighted in Fig. 4*a* and *b*. The starting chips showed grains as large as 100 µm. The GSD of the Al 7075 pulverised and atomised powders are presented in Fig. 5*a*. The pulverised powder displayed a definitively lower GSD than the starting chips. When compared to the atomised powder, the

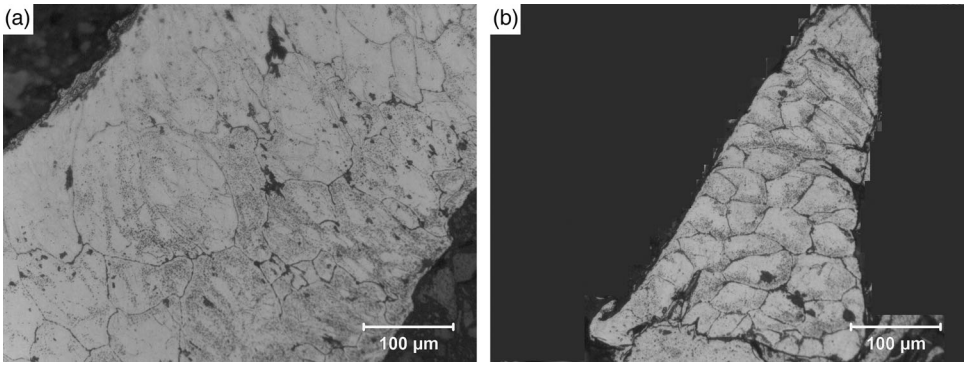


**4 Optical micrographs of the Al 7075 *a* chips and *b* pulverised powder, highlighting qualitatively the grain refinement occurring during comminution.**

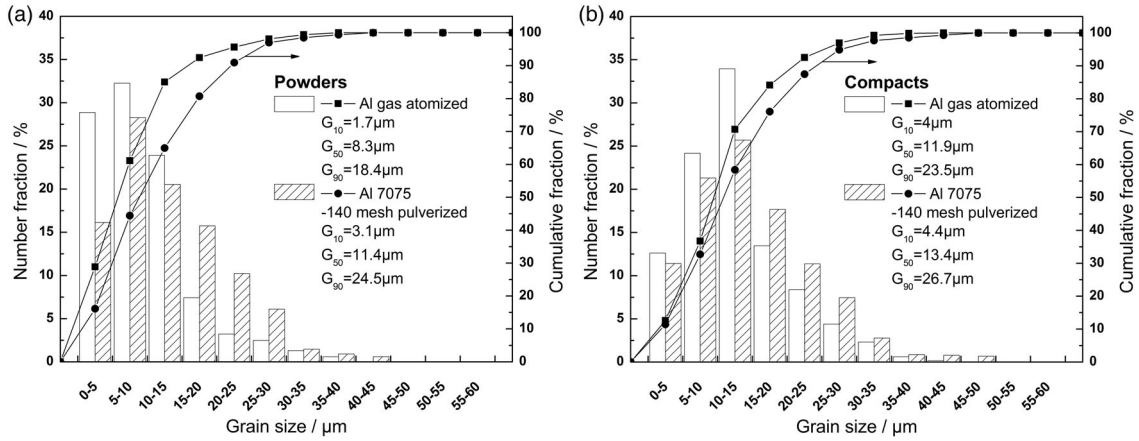


**5 GSD and cumulative frequency curves of the pulverised and atomised Al 7075 *a* powders and *b* SPS compacts**

pulverised powders have a larger grain size distribution, quantitatively confirmed by the reported $G_{10}$, $G_{50}$ and $G_{90}$ values. The GSD reported in Fig. 5 were obtained from measurements using optical micrographs of limited resolution. TEM observations, presented in Fig. 6*a* and *b*, were used to evaluate whether nanometre-sized grains were produced during comminution. The powder deformation mechanisms occurring upon milling suggest that

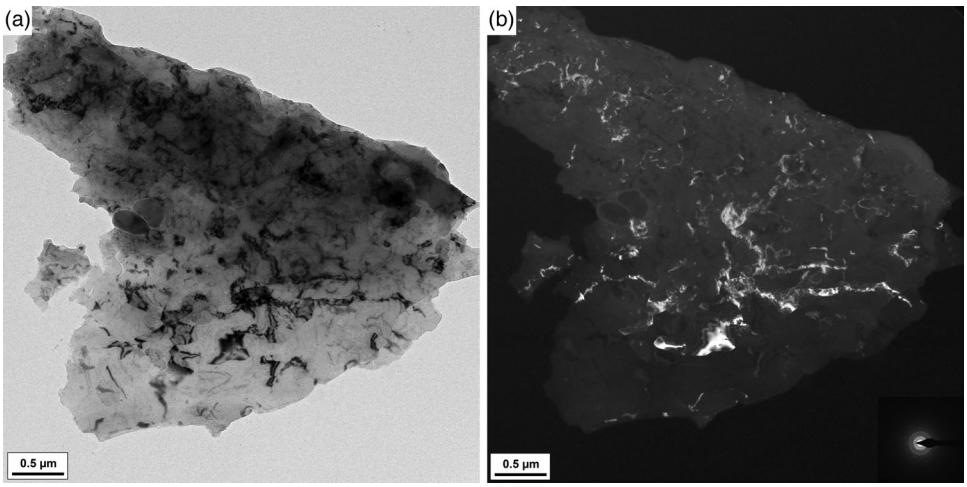


**6 *a* BF and *b* DF TEM micrographs (including SAED pattern), highlighting the presence of nanometre-sized grains in the Al 7075 pulverised powders**

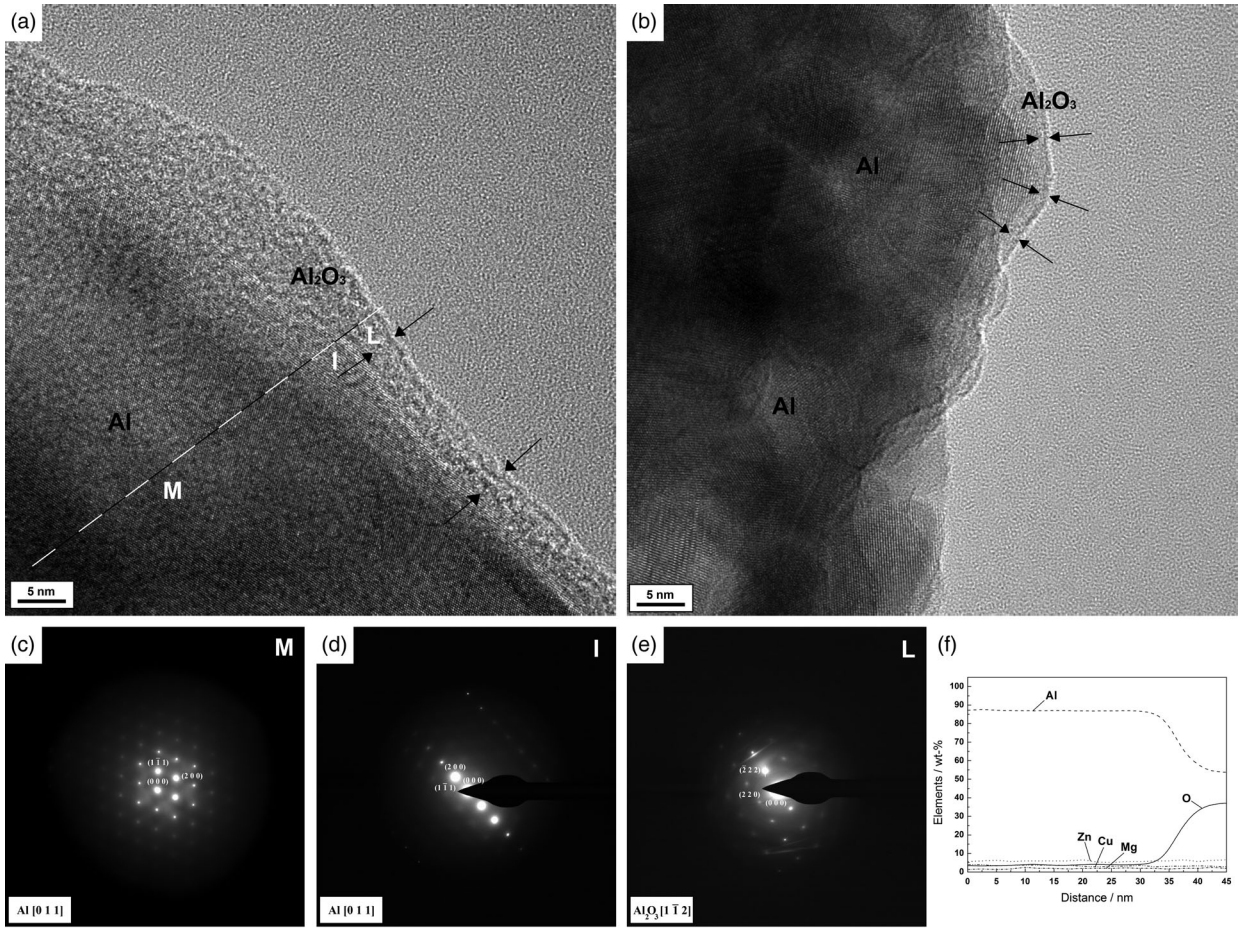


**7 Direct BF HRTEM observations of the passivation layer of the Al 7075 *a* pulverised and *b* gas atomised powders, with black arrows highlighting the oxide layer thickness. SAED patterns of the particle c matrix, *d* matrix-passivation layer interface and *e* passivation layer; the origin of each pattern, respectively labelled M, I and L, is indicated on the BF micrograph of the pulverised powder, as well as the *f* EDS linescan (dashed) from the particle matrix to the passivation layer**

the majority of the small grains should potentially be present near the surface of large particles while the core of such particles remains relatively coarse grained.[12] By combination of the results from optical microscopy and TEM, the microstructure of the pulverised powder is characterised by a bimodal grain size distribution, mainly composed of micrometre-sized grains accompanied with a relatively small fraction of nanometre-sized grains. The mechanical properties of the compacts sintered using this powder should be dictated by the micrometre-sized grains.[19,20]

The native Al passivation layer, contamination and matrix oxide particle content of the powders will also play key roles during sintering and in the mechanical response of the sintered compacts.

As such, the thickness of Al passivation layer was quantified for both the pulverised and atomised powders from the TEM observations shown, respectively, in Fig. 7*a* and *b*. The boundary between the powder matrix and the passivation layer was delimited using SAED patterns of the particle matrix (Fig. 7*c*), matrix-passivation layer interface (Fig. 7*d*) and passivation layer (Fig. 7*e*); the origin of these patterns was labelled, in Fig. 7*a*, as M, I and L. Fig. 7*c*, *d* and *e* highlights the gradual transition from the Al crystal structure to the oxide passivation layer structure. In particular, Fig. 7*d* presents residual diffraction spots from the Al matrix structure which supports the structural change occurring at the interface between the particle matrix and the passivation

**Table 2 Passivation layer thickness, content of exogenous contaminants present in the powder and total oxygen content of the Al 7075 pulverised and atomised powders**

| Materials | Passivation layer thickness/nm | Exogenous contaminants/ wt-% | Total oxygen content/ wt-% |
|---|---|---|---|
| Al 7075 gas atomised powder | 2·3 ± 1·3 | N/A | 0·12 ± 0·01 |
| Al 7075 pulverised powder | 7·9 ± 0·6 | 1·90 ± 0·02 | 1·10 ± 0·01 |

layer. Moreover, in Fig. 7*f*, the EDS linescan of the pulverised powder carried out from the particle matrix to its surface highlighted the concomitant increasing oxygen concentration and decreasing aluminium concentration as the particle surface is reached. The latter results are consistent with the presence of an oxide layer and provided evidence to accurately determine the passivation layer thickness of these powders. Therefore, the recorded native oxide layer thicknesses of the pulverised and atomised powders were 7·9 ± 0·6 and 2·3 ± 1·3 nm, respectively. It should be noted that the oxide layer thickness corresponding to the onset of the decrease in oxygen concentration reported in Fig. 7*f* agrees with the previous result. The presence of Cu, Mg and Zn was also observed in the particle matrix and passivation layer in Fig. 7*f*.

Table 2 summarises the results quantifying the passivation layer thickness of both powders, the content of exogenous contaminants and the total oxygen content of the powders.

First, results from Table 2 show that the passivation layer thickness varies significantly between the atomised and pulverised powders. The gas atomised powder showed a 2·3 ± 1·3-nm thick passivation layer, from its low exposure to oxygen during processing. This is in good agreement with the results obtained in other studies.[21,22] However, the standard deviation of the oxide layer thickness is large and can be attributed to the inhomogeneous thickness of the native oxide layer observed in Fig. 7*b*. On the other hand, the Al 7075 pulverised powder exhibited a significantly thicker passivation layer of 7·9 ± 0·6 nm, attributed to the availability of virgin Al surfaces produced during deformation and oxidation upon contact with air. Bloch reported that the latter comminution-induced phenomena yielded powder particles having passivation layer thicknesses ranging from 5 to 15 nm.[22] Therefore, the reported passivation layer thickness for the pulverised powder agrees well with data presented in reference works.[21,22]

Second, in Table 2, the exogenous contaminants content was the summation of the production plant oxides contaminants, i.e. $K_2O$, $SiO_2$, CaO and $Fe_2O_3$, which were assumed to be the major oxide compounds present at the surface of the powder particles.

The reported contents of exogenous contaminants of each powder highlighted that the pulverised powder was more contaminated than the atomised powder. This contributes to the explanation of the higher total oxygen content observed for the pulverised powder.

Third, dispersion of $Al_2O_3$ particles in the powder matrix has been reported in both atomisation and comminution processes.[22,23] Atomised powder can typically contain between 0·5 and 1·5 wt-% of $Al_2O_3$ particles, while the $Al_2O_3$ particle content of pulverised powders ranges between 6 and 17 wt-%.[22] The latter observation further contributes to the difference in total oxygen content, noticed in Table 2, between the two powders.

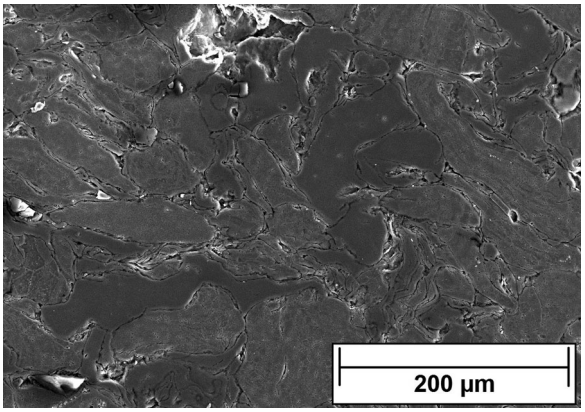


**8 SEM micrograph of the cross-section of Al 7075 pulverised powder compact highlighting the lack of interparticle bonding upon sintering**

## Sintering and compact characterisation

The GSD of the SPS compacts prepared from each powder are presented in Fig. 5*b*. In Fig. 5, the shift towards larger grain sizes is shown through the characteristic $G_{10}$, $G_{50}$ and $G_{90}$ values, while grain growth occurred to a lower extent in the pulverised alloy powder compared to the atomised powder during SPS. It is suggested that the presence of $Al_2O_3$ particles dispersed throughout the particle matrix and the native aluminium oxide-based layer could hinder the grain growth phenomenon by Zener pinning of the moving grain boundaries. This grain growth inhibition during SPS has already been reported.[24,25]

Table 3 presents a summary of the as-sintered density and mechanical response of the SPS compacts. For each powder, the selected sintering schedule yielded fully dense compacts, i.e. >99% of the theoretical density. The flexural strength of the pulverised powder compacts was 94·7 ± 7·2 MPa which is significantly lower than the flexural strength of 477·1 ± 15·1 MPa reported for the atomised powder compacts. This significant drop in strength cannot be solely ascribed to porosity, as the final density was in the same range.

The passivation layer on the Al particles surface has been reported to adversely affect powder consolidation by preventing the formation of metallurgical bonding between particles.[26,27] Such an effect of the passivation layer is evidenced in Fig. 8 upon sintering of the

**Table 3 Density, flexural strength and strain and hardness of the as-sintered SPS compacts of the Al 7075 pulverised and atomised powders**

| Materials | Density/% | Flexural strength/MPa | Flexural strain/% | Hardness/HV |
|---|---|---|---|---|
| Al 7075 gas atomised SPS compact | 99·9 ± 0·1 | 477·1 ± 15·1 | 4·2 ± 0·3 | 121·0 ± 3·7 |
| Al 7075 pulverised SPS compact | 99·0 ± 0·3 | 94·7 ± 7·2 | 2·1 ± 0·3 | 69·3 ± 5·2 |

pulverised powders. Almost no interparticle bonding can be observed, supporting the conclusion that the Al passivation layer effectively hindered powder consolidation. Therefore, the thick passivation layer developed at the surface of the pulverised powder effectively prevented the powder particles from forming metal/metal bonding interfaces, which is the primary factor dictating the strength of sintered compacts.[26] In addition, the oxide layer disruption during SPS of the pulverised powder could yield dispersion of broken oxide debris near the bonding interfaces between the particles which could further induce embrittlement of the compact.[26] For pure Al powder, the oxide layer breakage (increased sintering) is promoted with applied loads and sintering temperatures increasing concomitantly from 10 to 50 MPa and from 0·5 to 0·9 of the melting temperature, respectively.[26] In binary Al–Mg alloy systems, the oxide layer is a composite, consisting of $Al_2O_3$ particles and MgO (at low sintering temperatures) or $MgAl_2O_4$ spinel (at high sintering temperatures). The effectiveness of the MgO formation for breaking the $Al_2O_3$ layer is well documented and used to improve the sintering response.[28] However, the development of the spinel layer has an adverse effect, imposing the need for a higher applied load for oxide breakage and thus reducing sinterability. Other studies on the native oxide layer composition of Al 7475 and 7075 alloys suggest the presence of this spinel layer, which also contained Zn as a substitutional element.[29,30] In that context, it is believed that higher pressure than what was utilised in this work, above the maximum strength of graphite, will be required to break the surface scale, if possible, considering the oxide thickening from the comminution process. In Table 3, the mechanical properties reported for the atomised powder compact suggest that the applied load and magnesium content were sufficient to break the oxide layer and promote densification. While the low mechanical properties reported for the pulverised powder compact suggest that the magnesium content and 50 MPa of applied pressure were insufficient to completely break the thick native oxide layer that prevented the formation of metal/metal bonding between sintering particles of pulverised Al 7075 powder. A previous study on the role of magnesium during aluminium powder sintering showed that the magnesium content of the powder required to contribute to the oxide layer breakage is especially dependent on the passivation layer thickness.[31] In this case, the oxide layer reduction reaction taking place on the pulverised powder surface could not compensate for the passivation layer thickening occurring during comminution. Hence, based on the results of atomised powder densification, the minimum magnesium content required for the formation of interparticle bonding, under identical conditions as the atomised powder, between the pulverised powder particles was estimated at 5–6 wt-% Mg, which cannot be achieved due to the chemical composition specifications of the Al 7075 alloy. In order to provide an alternative recycling route for the pulverised powder, the magnesium content could be controlled through blending of the atomised and pulverised Al 7075 powders. However, separate investigations are required to determine the fractions of each powder to be blended considering the difference in physical properties of each powder.

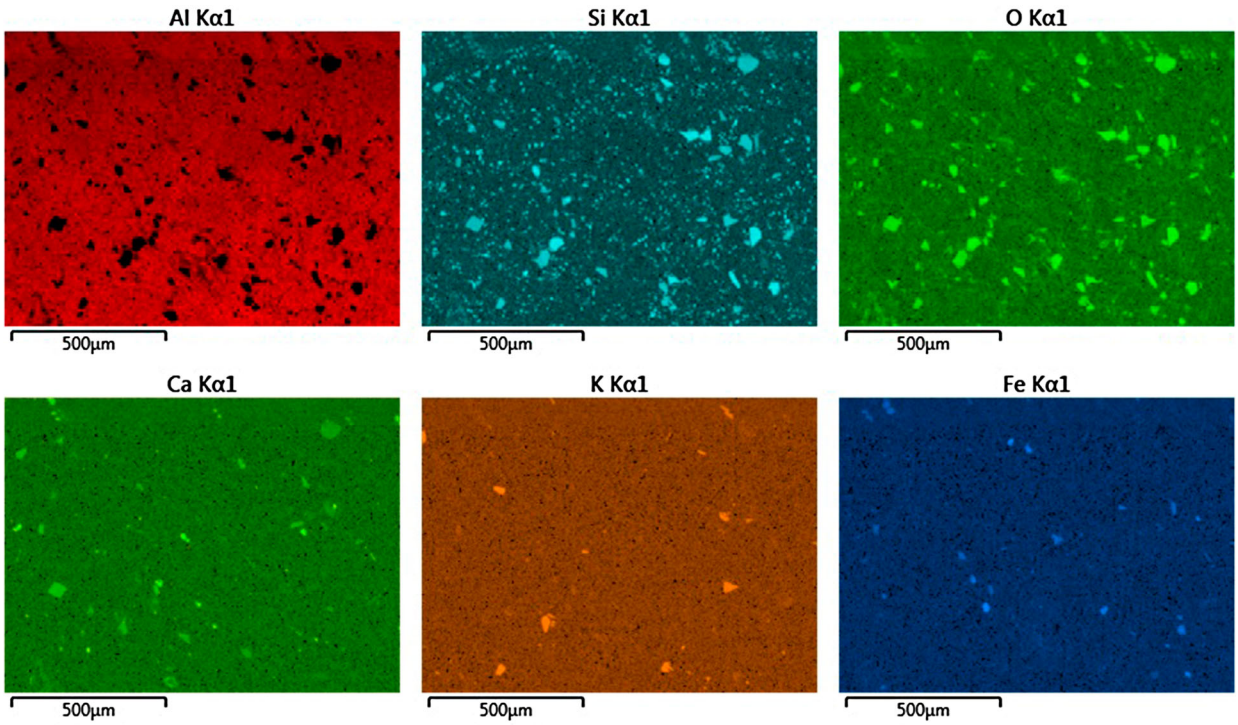


**9 EDS maps of the sintered Al 7075 pulverised powder compacts highlighting the presence of exogenous contaminants composed of silicon, calcium, potassium and iron oxides**

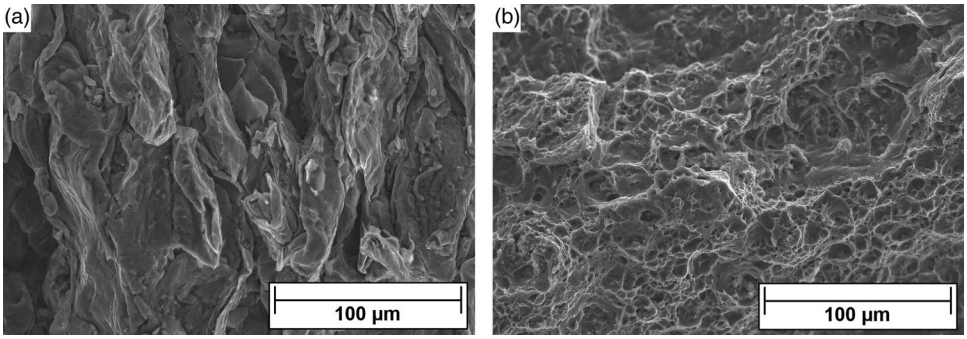


**10 Fracture surfaces of the sintered compacts of Al 7075 *a* pulverised and *b* atomised powders**

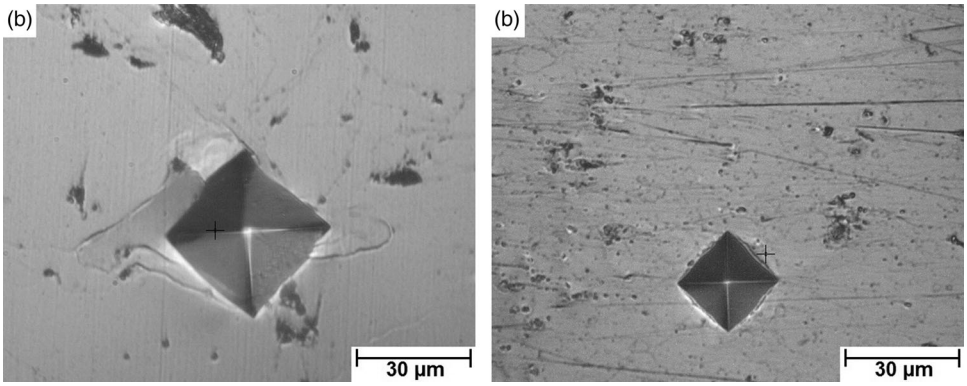


**11 Microhardness indents of the sintered compacts of Al 7075 *a* pulverised and *b* atomised powders**

Besides, it has been reported that pre-alloyed powders containing Mg and Zn were more hygroscopic than pure aluminium powders.[32] Their surface oxide film also includes both hydrated aluminium oxide ($Al(OH)_3$) and physically adsorbed water molecules layers.[33] In the absence of powder degassing, Al 7075 SPS compacts exhibited ~4% lower mechanical properties than their degassed powder compact equivalents, ascribed to poorer powder consolidation.[34] In addition, the low mechanical properties of the pulverised compacts can also be attributed to the presence of exogenous contaminants inherited from the feedstock chips. These contaminants were either embedded in the particle matrix or located at the particle boundaries as highlighted in Fig. 9 through the EDS maps of the as-sintered pulverised Al 7075 powder. They acted as crack nucleation and propagation sites instead of barriers to dislocation motion due to their relative incoherency with the matrix, further reducing the mechanical strength of the sintered compacts. It should be noted that the conversion of the surface fraction of the contaminants present in Fig. 9 agrees well with the oxygen content data reported in Table 2.

Fracture surfaces of pulverised and atomised powder compacts are presented in Fig. 10*a* and *b*, respectively. In Fig. 10*a*, the crack propagation occurred along the prior particle boundaries and no evidence of interparticle bonding was observed. Indeed, no dimples associated with ductile failure were found which supports the occurrence of particle debonding, while the fractured atomised powder compacts exhibited a significant presence of dimples (Fig. 10*b*). The higher extent of particle debonding occurring in the pulverised powder compact was further evidenced through the hardness indents micrographs presented in Fig. 11*a*. Indeed, significant particle debonding, associated with cracks originating from the sides of the indents, occurred during indentation of the pulverised powder compact while none was observed for the atomised powder compacts, as shown in Fig. 11*b*. This contributed to explain the low hardness value reported in Table 3 for the pulverised powder compact (69·3 ± 5·2 HV) compared to its atomised counterpart (121·0 ± 3·7 HV). It should be noticed that the indent size of Fig. 11*a* being larger than that of Fig. 11*b* also reflects the lower hardness value reported in Table 3 for the pulverised powder compact compared to its atomised counterpart.

Hence, the poor mechanical properties reported in Table 3 for the pulverised powder compacts are mainly attributed to its thicker oxide layer preventing interparticle bonding, the low magnesium content of the powder and to the presence of exogenous contaminants at the prior particle boundaries promoting particle debonding by acting as crack nucleation and propagation sites upon deformation. The results suggesting Al 7075 powder comminution for close-loop recycling towards the PM industry are currently not viable.

## Conclusions

This work studied a solid-state recycling route of Al 7075 chips consisting of a comminution process followed by direct consolidation of the pulverised powder using SPS. The pulverised powder presented a thick native oxide layer due to the extensive powder deformation inducing the exposure of virgin aluminium surfaces to air. The presence of exogenous contaminants, inherited from the feedstock chips, was highlighted and the total oxygen content of the powder suggested the existence of $Al_2O_3$ particle dispersion. The lack of sinterability of the powders was ascribed to deficient particle oxide layer breakage from the insufficient applied pressure (higher fracture strength from composite $Al_2O_3$/spinel layer), low magnesium content and potential degassing phenomenon. The low mechanical properties of the pulverised powder compacts resulted from the inhibition in the formation of metal/metal interparticle bonding during sintering. The presence of exogenous contaminants at prior particle boundaries facilitating particle debonding also plays a role in the drop in mechanical properties observed.

## Acknowledgements

The authors would like to thank the Consortium de Recherche et d'Innovation en Aérospatiale au Québec (CRIAQ), Bombardier, Bell Helicopter, Sotrem-Maltech, BFI, Nano Quebec, and Aluminerie Alouette for their project funding.

## References

1. S. K. Das: 'Recycling aluminium aerospace alloys', *Adv. Mater. & Process.*, 2008, 34–35.
2. J. A. S. Green: '*Aluminum recycling and processing for energy conservation and sustainability*'; 2007, Materials Park, OH, USA, American Society for Metals International.
3. T. G. Gutowski, J. M. Allwood, C. Herrmann, and S. Sahni: 'A global assessment of manufacturing: economic development, energy use, carbon emissions, and the potential for energy efficiency and materials recycling', *Ann. Rev. Environ. Resour.*, 2013, **38**, (1), 81–106.
4. R. L. Milford, J. M. Allwood, and J. M. Cullen: 'Assessing the potential of yield improvements, through process scrap reduction, for energy and $CO_2$ abatement in the steel and aluminium sectors', *Resour. Conserv. Recycl.*, 2011, **55**, (12), 1185–1195.
5. Y. Xiao and M. A. Reuter: 'Recycling of distributed aluminium turning scrap', *Min. Eng.*, 2002, **15**, (11, Suppl. 1), 963–970.
6. W. H. Geertruyden, C. A. Prescot, W. Z. Misiolek, and R. Peterson: 'Evaluation of light gauge Al scrap remelting after consolidation via the extrusion process', *Light Met. Age*, 2005, **63**, (6), 14–18.
7. D. K. Paraskevas, K., R. Renaldi, W. Dewulf, J.R. Duflou: 'Resource efficiency in manufacturing: identifying low impact paths', 10th Global Conf. on 'Sustain. Manuf.' (GCSM 2012), Istanbul, Turkey, 2012, 271–276.
8. V. Güley, N. B. Khalifa, and A. E. Tekkaya: 'Direct recycling of 1050 aluminum alloy scrap material mixed with 6060 aluminum alloy chips by hot extrusion', *Int. J. Mater. Form.*, 2010, **3**, (1), 853–856.
9. A. E. Tekkaya, M. Schikorra, D. Becker, D. Biermann, N. Hammer, and K. Pantke: 'Hot profile extrusion of AA-6060 aluminum chips', *J. Mater. Process. Technol.*, 2009, **209**, (7), 3343–3350.
10. J. B. Mann, S. Chandrasekar, W. D. Compton, K. P. Trumble, C. Saldana, S. Swaminathan, G. E. John, W. Moscoso, and T. G. Murthy: 'Severe plastic deformation and the production of nanostructured alloys by machining', in '*Nanostructured Metals and Alloys*', (ed. S. H. Whang), 178–210; 2011, Woodhead Publishing.
11. M. E. Schlesinger: '*Aluminum recycling*'; 2013, CRC Press.
12. C. Suryanarayana: 'Mechanical alloying and milling', *Prog. Mater. Sci.*, 2001, **46**, (1–2), 1–184.
13. Z. Sherafat, M. H. Paydar, and R. Ebrahimi: 'Fabrication of Al7075/Al, two phase material, by recycling Al7075 alloy chips using powder metallurgy route', *J. Alloys Compd.*, 2009, **487**, (1–2), 395–399.
14. T. Nagae, M. Yokota, M. Nose, S. Tomida, T. Kamiya, and S. Saji: 'Effects of pulse current on an aluminum powder oxide layer during pulse current pressure sintering', *Mater. Trans.*, 2002, **43**, (6), 1390–1397.
15. O. Guillon, J. Gonzalez-Julian, B. Dargatz, T. Kessel, G. Schierning, J. Räthel, and M. Herrmann: 'Field-assisted sintering technology/spark plasma sintering: mechanisms, materials, and technology development', *Adv. Eng. Mater.*, 2014, **16**, (7), 830–849.
16. 'Standard Test Methods for Metal Powders and Powder Metallurgy Products', MPIF, [s.l.], 2012.
17. 'Standard Test Method for Particle Size Distribution of Metal Powders and Related Compounds by Light Scattering', B822-02, ASTM International, West Conshohocken, PA, 2002.
18. D. Levasseur, S. Yue, and M. Brochu: 'Pressureless sintering of cold sprayed Inconel 718 deposit', *Mater. Sci. Eng., A*, 2012, **556**, 343–350.
19. M. A. Meyers, A. Mishra, and D. J. Benson: 'Mechanical properties of nanocrystalline materials', *Prog. Mater. Sci.*, 2006, **51**, (4), 427–556.
20. B. Q. Han, Z. Lee, D. Witkin, S. Nutt, and E. J. Lavernia: 'Deformation behavior of bimodal nanostructured 5083 Al alloys', *Metall. Mater. Trans. A*, 2005, **36**, (4), 957–965.
21. S. Özbilen, A. Ünal, and T. Sheppard: 'Influence of atomizing gases on the oxide-film morphology and thickness of aluminum powders', *Oxid. Met.*, 2000, **53**, (1–2), 1–23.
22. E. A. Bloch: 'Dispersion-strengthened aluminium alloys', *Metall. Rev.*, 1961, **6**, (1), 193–240.
23. J. S. Benjamin and M. J. Bomford: 'Dispersion strengthened aluminum made by mechanical alloying', *Metall. Trans. A*, 1977, **8**, (8), 1301–1305.
24. G. Sweet: 'Advanced sintering techniques of aluminum: spark plasma sintering', *MSc thesis*, Dalhousie University, NS, Canada, 2014.
25. B. Akinrinlola, R. Gauvin, and M. Brochu: 'Improving the mechanical reliability of cryomilled Al–Mg alloy using a two-stage spark plasma sintering cycle', *Scr. Mater.*, 2012, **66**, (7), 455–458.
26. G. Xie, O. Ohashi, M. Song, K. Furuya, and T. Noda: 'Behavior of oxide film at the interface between particles in sintered Al powders by pulse electric-current sintering', *Metall. Mater. Trans. A*, 2003, **34**, (3), 699–703.
27. R. M. German: '*Powder metallurgy & particulate materials processing*'; 2005, Princeton, NJ, USA, Metal Powder Industries Federation (MPIF).
28. G. Xie, O. Ohashi, M. Song, K. Mitsuishi, and K. Furuya: 'Reduction mechanism of surface oxide films and characterization of formations on pulse electric-current sintered Al–Mg alloy powders', *Appl. Surf. Sci.*, 2005, **241**, (1–2), 102–106.
29. J. Ryl, J. Wysocka, M. Jarzynka, A. Zielinski, J. Orlikowski, and K. Darowicki: 'Effect of native air-formed oxidation on the corrosion behavior of AA 7075 aluminum alloys', *Corros. Sci.*, 2014, **87**, 150–155.
30. S. K. Toh, D. G. McCulloch, J. Du Plessis, P. J. K. Paterson, A. E. Hughes, D. Jamieson, B. Rout, J. M. Long, and A. Stonham: 'An investigation of the native oxide of aluminum alloy 7475-T7651 using XPS, AES, TEM, EELS, GDOES and RBS', *Surf. Rev. Lett.*, 2003, **10**, (365), 365–371.
31. R. N. Lumley, T. B. Sercombe, and G. M. Schaffer: 'Surface oxide and the role of magnesium during the sintering of aluminum', *Metall. Mater. Trans. A*, 1999, **30**, (2), 457–463.
32. N. A. Plakhotnikova, V. G. Gopienko, A. A. Kolpachev, and G. A. Reznikova: 'Chemical reaction of aluminum alloy powders with water', *Sov. Powder Metall. Met. Ceram.*, 1988, **27**, (8), 605–608.
33. L. A. Arbuzova, V. A. Danilkin, and L. L. Kunin: 'Amount of $H_2O$ on the surface of an aluminum powde', *Sov. Powder Metall. Met. Ceram.*, 1976, **15**, (9), 663–665.
34. A. S. Chua, M. Brochu, and D. P. Bishop: 'Spark plasma sintering of prealloyed aluminium powders', *Powder Metall.*, 2014, **58**, (1), 51–60.